A&A 400, 249–256 (2003)
DOI: 10.1051/0004-6361:20021864

Astronomy & Astrophysics

X-ray spectroscopy of UZ Librae

P. Gondoin⋆

Space Science Department, European Space Agency – Postbus 299, 2200 AG Noordwijk, The Netherlands

Received 11 November 2002 / Accepted 16 December 2002

Abstract. UZ Librae is the giant primary of a close binary system with extremely fast rotation and revolution. Its distinctive characteristics include an optical light curve with a large amplitude and a high X-ray luminosity. UZ Librae was observed twice at five months interval in August 2000 and January 2001 by the *XMM–Newton* space observatory. Serie of lines of highly ionized Fe and several lines of the Ly and He series are visible in the reflection grating spectra, most notably from C, O and Ne. The corresponding ions are associated with plasma components with temperature in the range 3–8 MK. Bremstrahlung emission from plasma at high temperature ($T > 3 \times 10^7$ K) indicates an intense flaring activity on UZ Librae. This is also supported by a Ne abundance enhancement relative to oxygen reminiscent of abundance anomalies observed during stellar and solar flares. In contrast to oxygen and neon, the abundance of Fe in the corona of UZ Librae is determined to be a tenth of the solar photospheric value. We conjecture that the large fluid kinetic helicity induced by the rapid rotation of the star currently generates magnetic fields with two characteristic scales comparable with compact loops within solar active regions and with larger cooler loops interconnecting solar active regions. The X-ray emission of UZ Librae would be strongly enhanced not only due to the occurrence of these magnetic structures, but mainly due to their large surface coverage and to their permanent interactions responsible for heating UZ Librae plasma to high temperatures. A rotational modulation effect could have contributed to the luminosity variation between the two *XMM–Newton* observations since a large fraction of the X-ray emitting material might be located above large photospheric spots detected on Doppler images of the star.

Key words. stars: individual: UZ Librae – stars: activity – stars: coronae – stars: evolution – stars: late-type – X-rays: stars

1. Introduction

UZ Librae (BD-08°3999; $V = 9.11$) is the giant primary of a close binary system with an extremely fast rotation and revolution period of only 4.76 days. It is among the most active binary systems of the RSCVn class (Bopp & Stencel 1981). Dempsey et al. (1997) present X-ray observations of evolved binary systems including UZ Librae, obtained with the Position Sensitive Proportional Counter (PSPC) during the *ROSAT* All-Sky Survey phase of the mission. These authors convert count rates obtained in the 0.1–2.4 keV into X-ray fluxes and derive an upper limit of UZ Librae luminosity equivalent to $L_X < 10^{31}$ erg s^{-1} using the distance (≈140 pc) inferred from *Hipparcos* parallax (Perryman et al. 1997). This limit is consistent with a previous *Einstein* measurement (Drake et al. 1989) in the 0.2–3.5 keV band equivalent to $L_X \approx 5.3 \times 10^{30}$ erg s^{-1}. Wisniewski (1973) reported an IR excess and Bopp et al. (1984) tentatively suggested a dM companion. More recently, Olah et al. (2002) also favour a binary scenario where UZ Lib, a K0 giant, has a low mass secondary. The ultraviolet excess observed with *IUE* (Grewing et al. 1989) would then be explained by its very active chromosphere. The light curve of UZ Librae has been shown to display photometric amplitudes of up to 0.35 mag in V band. The Hα emission intensity and profile are variable over the rotation period. The strongest emission occurs at photometric minimum, in accord with the presence of cool starspots on the rapidly rotating K giant ($v \sin i \approx 90$ km s^{-1}; Bopp & Stencel 1981). Modelling photometric data, Olah et al. (2002) found a surprisingly well-defined phase coherence of the light curve minima for eight consecutive years. If interpreted as being due to spots, two main spotted regions centered at approximately 90° and 270° longitude were present at all times between 1993 and 2001. We report on analysis results of X-ray spectra of UZ Librae registered during two observations performed in August 2000 and January 2001 by the *XMM–Newton* observatory. This work aims to improve our understanding of the magnetic activity on UZ Librae by investigating the origin of its high X-ray luminosity.

2. Observations and data reduction

UZ Librae was observed twice by the *XMM–Newton* space observatory (Jansen et al. 2001), respectively in revolution 127 on 2000 August 19 and in revolution 210 on 2001 January 31 (see Table 1). The satellite observatory uses three grazing incidence telescopes which provide an effective area higher than 4000 cm^2 at 2 keV and 1600 cm^2 at 8 keV (Gondoin et al. 2000). Three CCD EPIC cameras (Strüder et al. 2001; Turner et al. 2001) at the prime focus of the telescopes provide imaging in a 30 arcmin field of view and broadband spectroscopy

⋆ e-mail: pgondoin@rssd.esa.int

Table 1. UZ Librae observation log during revolutions 127 and 210.

Rev.	Experiment	Filter	Mode	Start Exp. (UT)	Exp. Duration
	MOS1	Medium	Full frame	2000-08-19@04:53:28	27174 s
	MOS2	Medium	Full frame	2000-08-19@04:53:28	27174 s
127	$p-n$	Medium	Full frame	2000-08-19@05:34:53	24468 s
	RGS1		Spec + Q	2000-08-19@04:45:02	29956 s
	RGS2		Spec + Q	2000-08-19@04:45:02	29956 s
	MOS1	Medium	Full frame	2001-01-31@19:29:53	27524 s
	MOS2	Medium	Full frame	2001-01-31@19:29:53	27524 s
210	$p-n$	Medium	Full frame	2001-01-31@20:11:16	25418 s
	RGS1		Spec + Q	2001-01-31@19:21:27	30256 s
	RGS2		Spec + Q	2001-01-31@19:21:27	30256 s

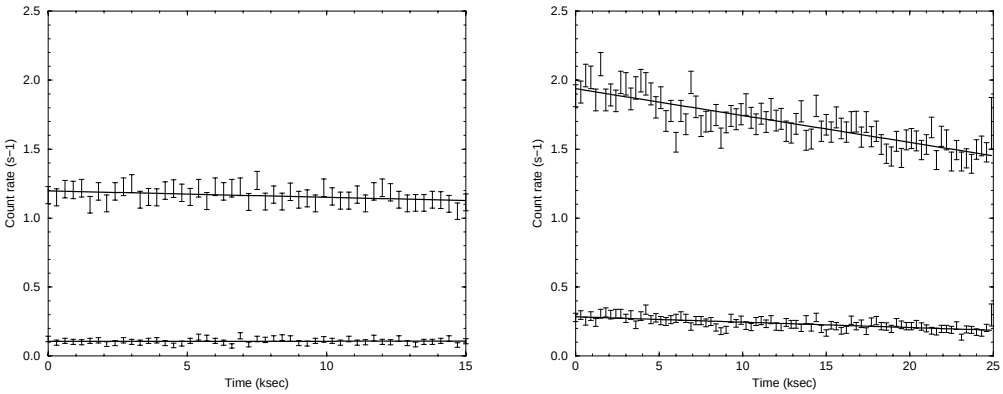

Fig. 1. Light curves of UZ Librae during revolutions 127 (left) and 210 (right) obtained with the EPIC $p-n$ camera. In each graph, the upper curve is the count rate in the 0.3 to 2 keV band and the lower curve is the count rate in the 2 to 10 keV band. The events are binned in 300 s time intervals.

with a resolving power of between 10 and 60 in the energy band 0.3 to 10 keV. Two identical RGS reflection grating spectrometers behind two of the three X-ray telescopes allow higher resolution ($E/\Delta E$ = 100 to 500) measurements in the soft X-ray range (6 to 38 Å or 0.3 to 2.1 keV) with a maximum effective area of about 140 cm^2 at 15 Å (den Herder et al. 2001). UZ Librae observations were conducted with the EPIC cameras operating in full frame mode (Ehle et al. 2001). RGS spectra were recorded simultaneously. Optical/UV observations were also performed with the 30 cm Optical Monitor (OM) aboard *XMM–Newton* (Mason et al. 2001) using a UV filter and a low resolution visible grism. "Medium" thickness aluminum filters were used in front of all EPIC cameras to reject visible light from the star itself. Processing of the raw event dataset was performed using the "emchain", "epchain" and "rgsproc" pipeline tasks of the *XMM–Newton* Science Analysis System (SAS version 5.3.0). UZ Librae spectra were built from photons detected within a window of about 50″ diameter around the target boresight in the MOS cameras. A smaller 39″ diameter extraction window was used for the $p-n$ data imposed by the proximity of the $p-n$ CCD edges. The background was estimated on the same CCD chips as the source, within windows of the same sizes which were offset from the source position in an empty field region. The SAS task "epatplot" was used to verify that the count rate of the target does not produce pile-up effect in the core of the telescope point spread function registered by the EPIC cameras. The Pulse-Invariant (PI) spectra were rebinned such that each resulting MOS channel had at least 20 counts per bin and each $p-n$ channel had at least 50 counts per bin. χ^2 minimization was used for spectral fitting. All fits were performed using the XSPEC package (Arnaud & Dorman 2001). The EPIC and RGS response matrices were generated by the SAS task "rmfgen" and "rgsrmfgen" respectively. EPIC $p-n$, MOS 1 and MOS 2 spectra were fitted together in the 0.3 to 10 keV energy range. The RGS spectra were analysed separately due to their higher spectral resolution in the 0.3−2.1 keV energy range.

3. Integrated flux and temporal behaviour

Figure 1 shows the light curves of UZ Librae obtained during revolutions 127 and 210 with the $p-n$ camera. Due to a rising background towards the end of the exposure, the analysis of revolution 127 data was limited to the first 15 ksec of the observation. The count rate was about 50% higher in revolution 210 with an average count rate of 1.69 ± 0.23 s^{-1} compared with a count rate of 1.15 ± 0.03 s^{-1} in revolution 127. The 2–10 keV over 0.3–2 keV count rate ratios were respectively 0.086 ± 0.02 and 0.137 ± 0.07 during revolutions 127 and 210 respectively, indicating that the spectrum of UZ Librae was harder during the second observation in January 2001. The X-ray flux was slightly variable during both observations. The count rate in the low energy band decreased steadily by 5.3% within 15 ksec and by 14% within 25 ksec during revolution 127 and 210, respectively.

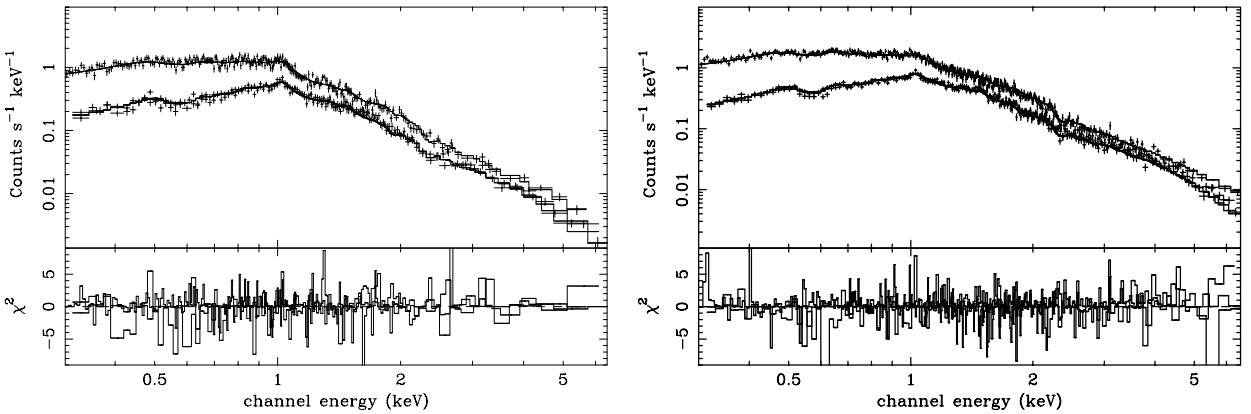

Fig. 2. Best fit models to revolution 127 (left) and to revolution 205 (right) spectra. The EPIC data (crosses) and spectral fit (solid line) are shown in the upper panel and the χ^2 contributions in the lower panel of each graph.

Table 2. X-ray fluxes of UZ Librae in the 0.3−2 keV and 2−10 keV energy bands averaged over the different observations and corrected for interstellar absorption. The percentage contribution in flux of hot plasmas ($kT > 3$ keV) is indicated between bracketts.

Obs.	$F_{0.3-2\ \mathrm{keV}}$ (10^{-12} erg cm^{-2} s^{-1})	$F_{2-10\ \mathrm{keV}}$ (10^{-12} erg cm^{-2} s^{-1})	hr
Rev. 127	4.2	1.2	−0.54
	(25%)	(60%)	
Rev. 210	6.2	3.0	−0.35
	(49%)	(82%)	

The spectral analyses of each observation were conducted separately. Spectral fitting of the EPIC data (see Sect. 4) during these two periods yields flux measurements (see Table 2) in the 0.3−2 keV and 2−10 keV bands. Table 2 also provides the hardness ratio hr of the X-ray emission defined as $hr = (F_{2-10\ \mathrm{keV}} - F_{0.3-2\ \mathrm{keV}})/(F_{2-10\ \mathrm{keV}} + F_{0.3-2\mathrm{keV}})$ which indicates that the X-ray spectrum of UZ Librae was harder during revolution 210. Compared with revolution 127, the X-ray flux of UZ Librae during revolution 210 was 50% and 240% higher in the 0.3–2 keV and 2–10 keV band, respectively.

4. Spectral analysis of EPIC data

The two EPIC datasets (see Fig. 2) were fitted separately with the MEKAL optically thin plasma emission model (Mewe et al. 1985). The spectral fitting was performed in the 0.3–7 keV and 0.3–10 keV spectral bands for revolution 127 and 210, respectively since revolution 127 data does not contain any significant signal above 7 keV. The interstellar hydrogen column density was fixed to $N_{\mathrm{H}} = 8.7 \times 10^{20}$ cm^{-2} (Dickey & Lockman 1990). No single or two temperature plasma model that assumes either solar photospheric (Anders & Grevesse 1989) or non solar abundances can fit the data, as unacceptably large values of χ^2 were obtained. MEKAL plasma models with three components at different temperatures gives marginable acceptable fits with reduced χ^2 of 1.21 and 1.17 for revolution 127 and 210, respectively. An improvement in χ^2 statistic to the fit is obtained by adding a fourth temperature component. The improvements in χ^2 fit statistics ($\Delta\chi^2/\Delta\nu = 10$ for 578 degrees of freedom in revolution 127 and $\Delta\chi^2/\Delta\nu = 6$ for 932 degrees of freedom in revolution 210) are significant at >90% confidence using the F-statistic. The best fit models are described in Table 3. The emission measure is displayed as a function of temperature in Fig. 3 which shows that the emission measure peaks at about 1 keV in revolution 127. In revolution 210, the maximum emission measure contribution comes from plasma hotter than 3 keV. The EPIC data were also fitted using the column density as a free parameter. The result does not change but constrains the absorption column density to $N_{\mathrm{H}} = (8.5 \pm 0.7) \times 10^{20}$ cm^{-2} in agreement with Dickey & Lockman (1990).

Table 3. Best fit parameters to EPIC data using a 4 component MEKAL model (Mewe et al. 1985) and an hydrogen column density of 8.7×10^{20} cm^{-2}. The spectral fitting was conducted in the 0.3–7 keV and 0.3–10 keV for revolution 127 and revolution 210 respectively, with the same abundance relative to the Sun for all components.

	Rev. 127	Rev. 210
Z	0.10 ± 0.01	0.10 ± 0.01
kT_1 (keV)	0.19 ± 0.02	0.24 ± 0.02
EM_1 (10^{52} cm^{-3})	31 ± 7	51 ± 6
kT_2 (keV)	0.56 ± 0.05	0.67 ± 0.08
EM_2 (10^{52} cm^{-3})	29 ± 6	18 ± 8
kT_3 (keV)	1.13 ± 0.05	1.23 ± 0.06
EM_3 (10^{52} cm^{-3})	82 ± 15	33 ± 12
kT_4 (keV)	3.2 ± 0.5	3.7 ± 0.3
EM_4 (10^{52} cm^{-3})	37 ± 14	90 ± 12
χ^2	681/578 d.o.f. = 1.18	1076/932 d.o.f. = 1.16

Hot ($T > 3$ keV) plasma in UZ Librae corona is a major source of X-ray emission both in the soft and in the hard X-ray band. It contributes to more than 25% of the soft X-ray luminosity in the 0.3−2 keV range and to more than 60% of the luminosity above 2 keV (see Table 2). The X-ray luminosity variation of UZ Librae both in the soft (<2 keV) and in the hard (>2 keV) spectral range are mainly related to change in the emission measure of this hot ($T > 3$ keV) plasma. It increased by more than a factor of 2 between revolution 127 and 210 (see Table 3). Assuming identical abundances in the four plasma components, the average element abundance in UZ

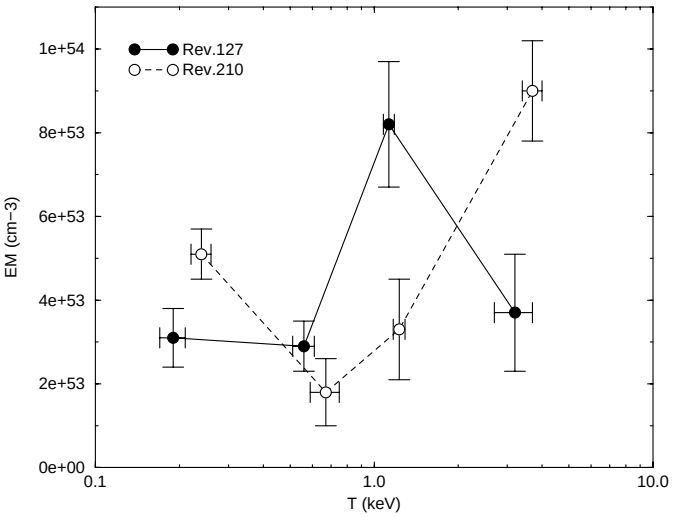

Fig. 3. Emission measure of different plasma components in UZ Librae corona as a function of temperature in revolutions 127 and 210.

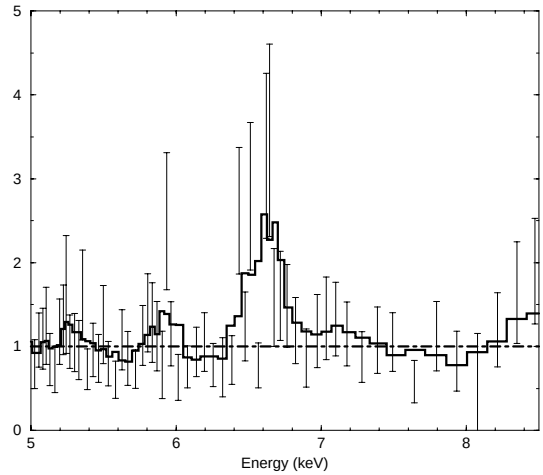

Fig. 4. Ratio of UZ Librae spectrum obtained during revolution 210 to the best fit power law model in the 4.5–10 keV range.

Librae corona is found to be lower than the solar photospheric value (see Table 3).

One major feature of UZ Librae spectrum during revolution 210 is the presence of a high energy tail. An emission feature around 6.5 keV attributed to an iron K emission line (see Fig. 4) could be present in revolution 210 but is not detected in revolution 127. The iron Kα fluorescence line consists of two components Kα_1 and Kα_2 at 6.404 keV and 6.391 keV respectively for Fe I and a branching ratio of 2:1 (Bambynek et al. 1972). The natural width of the lines ($\Delta E \approx 3.5$ eV) and any broadening due to thermal motions of the emitting atoms ($\Delta E(\mathrm{eV}) \approx 0.4(T/10^6)^{1/2}$) are negligible compared to the energy resolution (155 eV FWHM) of the EPIC cameras. The iron Kα fluorescent line energy is an increasing function of the ionization state. It rises slowly from 6.40 keV in Fe I to 6.45 keV in Fe XVII (neon-like) and then increases steeply with the escalating number of vacancies in the L-shell to 6.7 keV in Fe XXV and 6.9 keV in Fe XXVI (House 1969; Makishima 1986). Spectral fits to the EPIC $p-n$ spectra above 4 keV by a powerlaw and a Gaussian line model give a power law with a slope $\Gamma = 2.9 \pm 0.2$ and an Fe K line at 6.46 ± 0.11 keV with an equivalent width $EW \approx 45$ eV. This result suggests the presence of iron in intermediate states of ionization during revolution 210 but the improvement of the power law fit with an additional Gaussian line component is not significant ($\Delta\chi^2 = -0.4$ for 116 degree of freedom).

5. Spectral analysis of RGS data

Figure 5 shows the RGS spectra averaged over revolution 127 and over revolution 210. Each spectrum is the sum of the two spectra simultaneously obtained with the RGS1 and RGS2 reflection grating spectrometers on board *XMM–Newton*. For line identification, we required only that the wavelength coincidence be comparable to the spectral resolution of the RGS spectrometers, namely 0.04 Å over the 5 to 35 Å wavelength range. In the X-ray domain, many candidate lines may exist within this acceptable wavelength coincidence range. Hence, we only looked for resonance transitions of abundant elements and predicted line intensities using spectra of the Sun (Doschek & Cowan 1984) and of Capella (Brinkman et al. 2000). Serie of lines of highly ionized Fe and several lines of the Ly and He series are visible in RGS spectra, most notably from C, O and Ne. The strongest lines are listed in Table 4. Their temperatures of maximum formation range between 1 and 8 MK indicating that the corresponding ions are associated with the cool plasma components inferred from EPIC data.

When comparing the spectra obtained during revolution 127 and 210, the most obvious difference is the higher continuum emission observed at short wavelengths during revolution 210. This continuum is mainly associated with the bremstrahlung emission from the high temperature ($T > 3 \times 10^7$ K) plasma derived from EPIC data which most contributes to the overall X-ray luminosity of UZ Librae during revolution 210. Line fluxes were measured using XSPEC by fitting the RGS spectra with Gaussian profiles, which represent the observed line profiles very well. Line fluxes are given in Table 4. Flux measurements of the Ne X (12.13 Å) and O VIII (16.01 Å) lines are affected by blends. Difference of line intensities are seen between revolutions 127 and 210. The lack of Al XIII and C VI detection is attributed to the lower signal to noise ratio of revolution 127 dataset. The intensity of the O VIII lines was significantly higher (by a factor of 2) during revolution 210.

We fitted the low energy RGS spectra obtained in revolution 127 and 210 by a single temperature VMEKAL model with variable abundances. The model generates a spectrum of hot diffuse gas with line emission from several elements based on the calculation of Mewe et al. (1985) with Fe L calculations by Liedahl (1995). A single electron temperature and electron density is assumed for the entire ensemble of element charge states and in particular for iron, oxygen and neon which produce the most prominent lines. This highly simplified assumption turns out to be fairly adequate within the observational uncertainties of the present spectrum. The fit was performed in the spectral range from 10 Å to 20 Å where the efficiency of the RGS spectrometers is the highest. The continuum emission of the hot plasma component was modelized by a bremstrahlung

Table 4. Measured positions and fluxes of the strongest lines in the RGS spectra of UZ Librae obtained during revolutions 127 and 210. The columns give the predicted line positions, the measured line positions during revolution 127, the measured line positions during revolution 210, the ion and line identifications, the temperatures of maximum line formation, the line fluxes measured during revolution 127 and the line fluxes measured during revolution 210.

$\lambda_{\rm pred}$ (Å)	$\lambda_{\rm rev127}$ (Å)	$\lambda_{\rm rev210}$ (Å)	Ion	line ID	$\log(T_{\rm m})$ log (K)	$F_{\rm rev127}$ (10^{-6} cm^{-2} s^{-1})	$F_{\rm rev210}$ (10^{-6} cm^{-2} s^{-1})
7.17		7.17	Al XIII	Lyα1,2			77 ± 20
10.70		10.66	Fe XIX	3F3	6.90		85 ± 15
12.13	12.14	12.13	Ne X	H1AB	6.80	86 ± 14	111 ± 17
12.12	(b)	(b)	Fe XVII	4C	6.75	(b)	(b)
13.45	13.45	13.45	Ne IX	He4w	6.60	41 ± 13	63 ± 15
16.01	16.04	16.01	O VIII	H2	6.60	26 ± 12	53 ± 13
16.07	(b)	(b)	Fe XVIII	F3	6.80	(b)	(b)
18.97	18.98	18.98	O VIII	H1AB	6.50	49 ± 14	115 ± 18
33.74		33.76	C VI	H1AB	6.10		123 ± 27

Table 5. Best fit parameters to RGS spectra in the 0.6–1.3 keV range recorded in revolution 127 and 210 using a VMEKAL model with variable O and Ne abundances.

Model	Parameter	Rev. 127	Rev. 210
WABS	$n_{\rm H}$ (cm^{-2})	8.7×10^{20}	8.7×10^{20}
BREMS	kT (keV)	3.2	3.7
	kT (keV)	0.72 ± 0.05	0.69 ± 0.06
VMEKAL	O	0.5 ± 0.2	0.8 ± 0.2
	Ne	1.7 ± 0.6	1.9 ± 0.7
	Other abundances	0.1	0.1
	χ^2	1.10 (310/282)	1.04 (347/333 d.o.f)

component at a temperature of 3.2 keV (revolution 127) and 3.7 keV (revolution 210) as derived from spectral fitting of EPIC data. The bremstrahlung model was normalised on the overall RGS spectral range. An initial abundance of 0.1 was used, as established by the MEKAL model applied to EPIC data. The temperature and abundances of the O and Ne elements which give prominent lines in the considered spectral range were then allowed to vary. The fitting results are given in Table 5. They indicate that the plasma responsible for the line emission has a peak temperature around 0.7 keV. This is reminiscent of the emission measure distribution found from the EUV observations of Capella (G1 III + G8 III) (Dupree et al. 1993; Schrijver et al. 1995; Brickhouse et al. 2000). It is worth noting that *Chandra* observations (Behar et al. 2001) have also shown that the iron-L spectrum of Capella between 10 Å and 18 Å can be reproduced almost entirely by assuming a single electron temperature of $kT = 0.6$ keV. The single temperature simplification is apparently a reasonable modeling assumption for the soft X-ray emission line spectra of active giants. The O and Ne abundances are much higher than the average metallic abundance ($Z = 0.1$) derived from EPIC data. The Ne abundance is a factor of 2 to 3 higher than the O abundance. Hence, the Ne/O ratio found for UZ Librae is unusually high compared with the solar photospheric value. This Ne enhancement is reminiscent of a similar anomaly observed in a subset of solar flares (Murphy et al. 1991; Schmelz 1993). The results also suggest that the oxygen abundance is variable and was higher during revolution 210 than during revolution 127.

An information on the emitting volume of the different plasma components could be derived if their electron densities were known. Electron densities can be measured using density sensitive spectral lines originating from metastable levels, such as the forbidden (f) 2^3S-1^1S line in helium like ions. This line and the associated resonance (r) 2^1P-1^1S and intercombination (i) 2^3P-1^1S lines make up the so-called helium like triplet lines (Gabriel & Jordan 1969; Pradhan 1982; Mewe et al. 1985). The intensity ratio $(i+f)/r$ varies with electron temperature and the ratio i/f varies with electron density due to the collisional coupling between the metastable 2^3S upper level of the forbidden line and the 2^3P upper level of the intercombination line. The RGS wavelength band contains the He-like triplets from O VII, Ne IX, Mg XI and Si XIII. However, the Si, Mg and O triplets are not detected and the Ne IX triplet is too heavily blended with iron and nickel lines for unambiguous density analysis.

6. Discussion

The large throughput of the *XMM–Newton* telescopes enables to perform X-ray spectroscopy of UZ Librae corona, to derive characteristic temperatures and emission measures of different plasma components and to measure accurately X-ray fluxes. The luminosities in the 0.3–2.0 keV band derived using *Hipparcos* parallax ($L_{0.3-2\,\rm keV} = 9.8 \times 10^{30}$ erg s^{-1} and 14.6×10^{30} erg s^{-1} in revolution 127 and 210, respectively) are comparable with estimates ($L_{\rm X} \approx 5.3 \times 10^{30}$ erg s^{-1}) from *Einstein* (Drake et al. 1989) and *ROSAT* (Dempsey et al. 1997)

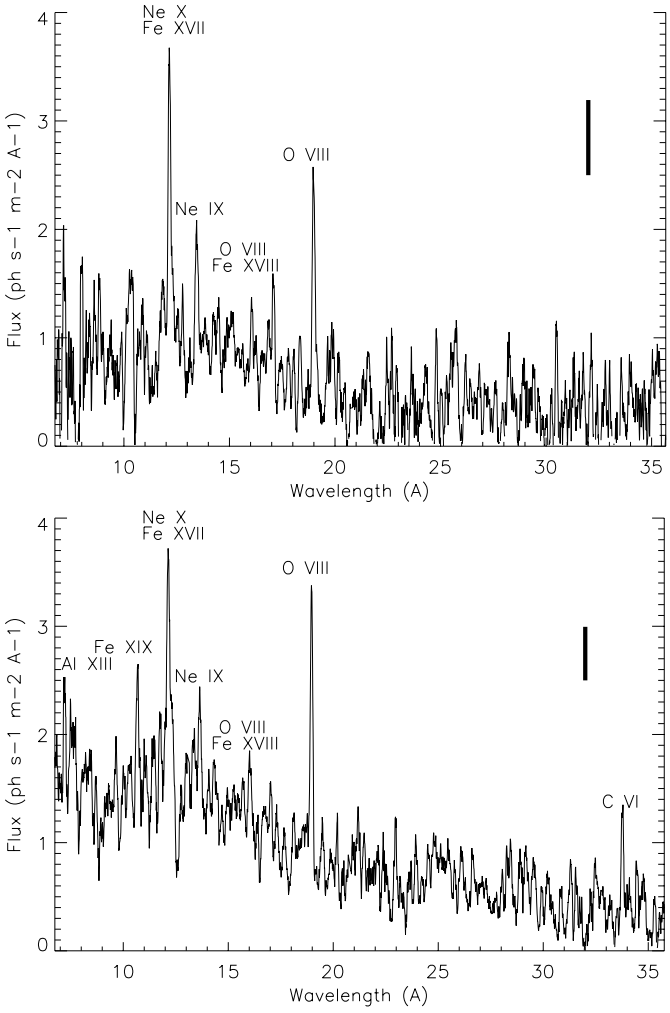

Fig. 5. Averaged first order spectra of RGS 1 and 2 obtained during revolutions 127 (top) and 210 (bottom). Typical error bars are indicated in the upper right corner of each graph. The absence of Al XIII and C VI detection in revolution 127 (top) is attributed to a lower signal to noise ratio.

count rate measurements (see Sect. 1). The EPIC cameras also measured significant X-ray emission above 2 keV ($L_{>2\,\mathrm{keV}}$ = 2.9×10^{30} erg s^{-1} and 7.0×10^{30} erg s^{-1} in revolution 127 and 210, respectively). The spectral fitting of the EPIC spectra of UZ Librae with a four component model suggests a corona configuration with little contribution from quiet regions similar to the Sun. On the contrary the 0.2–0.7 keV temperatures of the "cool" components is reminiscent of solar type active regions, while the hot ($T > 3$ keV) component may be caused by disruptions of magnetic fields associated to a permanent flaring activity. The review of coronal activity by Vaiana & Rosner (1978) pointed out that the Sun, if completely covered with active regions, would have an X-ray luminosity of 2×10^{29} ergs s^{-1}. When scaled to the surface of UZ Librae primary ($R \approx 8.2\ R_\odot$; Olah et al. 2002), an X-ray luminosity of 7×10^{30} erg s^{-1} is obtained assuming no X-ray contribution from the secondary star. This value is lower than the observed luminosity of UZ Librae (13 to 22×10^{30} erg s^{-1}) derived using Hipparcos parallaxes but comparable with the X-ray

Table 6. Physical parameters of UZ Librae coronal loops.

T (K)	EM (cm^{-3})	L (cm)	n (cm^{-3})
2.2×10^6	31×10^{52}	2×10^8	6.5×10^{10}
6.5×10^6	29×10^{52}	1.5×10^{10}	7.3×10^9

luminosity contribution (≈8–9 × 10^{30} erg s^{-1}) of its "cool" ($T < 3$ keV) plasma components. Following a simple rule of thumb, an UZ Librae surface almost entirely covered with bright solar like active regions could probably explain the X-ray luminosity of its "cool" ($T < 3$ keV) plasma components. Assuming that these component are produced by simple static loop systems each consisting of similar loops of constant pressure p (dyn cm^{-2}), temperature T (K) and cross section A (cm^2), the emission measure EM (cm^{-3}) can be expressed as:

$$EM = GF \times (4\pi R^2) \times (p/2kT)^2 \times L \quad (1)$$

where R is the stellar radius, F is the filling factor and L the loop half-length. G is a geometry factor which includes effect of partial occultation of the corona by the star itself (i.e. G varies from 0.5 to 1 for $L << R$ to $L >> R$). Using the relation $T = 1400(pL)^{1/3}$ (Rosner et al. 1978) and $G = 0.7$, a characteristic loop length scale is obtained (Mewe et al. 1982):

$$L_{10} = 7.4 \times F \times T_7^4 \times EM_{52}^{-1} \times (R/R_\odot)^2 \quad (2)$$

where L_{10} is the loop half length in units of 10^{10} cm, T_7 is the coronal temperature in unit of 10^7 K, and EM_{52} is the emission measure in units of 10^{52} cm^{-3}. Inserting the observed temperature and emission measures (see Table 3) of the cold ($T < 1$ keV) components, we derive the corresponding values of loop base pressures and half-lengths assuming a 50% filling factor (see Table 6). This simple analysis suggests the possible existence of two loop systems in the coronae of UZ Librae reminiscent of solar coronal loops. Indeed, solar corona observations show bright hot loops within active regions which reach maximum temperatures and electron densities above the neutral line of typically 3–4 × 10^6 K and 10^{10} cm^{-3} (Vaiana et al. 1973). In addition to these hot loops, on-disk images of the Sun show that neighboring active regions are often connected into complexes of activity by large loop-like structures (van Speybroek et al. 1970). These interconnecting loops can be >10^{10} cm long and tend to be cooler than loops within solar active regions.

With the straightforward deduction that in UZ Librae, the cool plasma components are produced by solar like active regions covering a large fraction of the star's surface, it is easy to imagine that such a dense population of active regions coexists with constant interaction and disruption of their magnetic fields which might be expected to lead to continuous flaring. This could explain the permanent emission measure of hot plasma above 1 keV. High temperature plasmas constitute flare indicators which have been detected from the Sun and from non-solar coronae (van den Oord & Mewe 1989; Tsuru et al. 1989). The solar flare plasma shows a bimodal temperature distribution with plasma at two different temperature 0.4–0.7 keV and

1.4–2.2 keV where the hot component is present only during the flares (Antonucci & Dodero 1995). The two components probably have a common origin in the flaring region on the Sun, since the componant at 0.4–0.7 keV cools to active region temperatures of 0.2–0.3 keV during the flare decay (Antonucci & Dodero 1995). The temperature of these components are remarkably close to the temperatures found in the X-ray emission from UZ Librae and other RSCVn systems. Intense flaring activity on UZ Librae is supported by a Ne abundance enhancement relative to oxygen reminiscent of abundance anomalies observed during stellar and solar flares. In contrast to oxygen and neon, the abundance of Fe in the corona of UZ Librae is determined to be a tenth of the solar photospheric value.

Although suggestive, the above interpretation does not take into account the complexity of UZ Librae geometry including the possible contribution of the secondary companion to the X-ray luminosity and the inhomogeneous structure of UZ Librae atmosphere indicated by the presence of large photospheric spots (Strassmeier 1996). Doppler images presented by Olah et al. (2002) suggest prefered spot locations for at least seven years between 1993 and 2001 onto the surface of UZ Librae primary star. According to these maps, two equatorial active regions are facing towards and opposite the unseen companion star. A large and cool polar spot, with two or may be three appendages extending down to a latitude of 40°–50° is also present. We used the orbital elements in Fekel et al. (1999; HJD = 2449993.62 + 4.768241 × E) to calculate the orbital phase of UZ Librae during *XMM–Newton* observations. The observation in revolution 127 was conducted near the time of conjonction with the primary star in front of the observer. The observation in revolution 210 was conducted near the time of quadrature with the secondary star receding. Hence, the coronal regions above the two equatorial spots at limb and above the polar spot may have been simultaneously visible during revolution 210. According to this geometry, only the polar region and one equatorial region on the disk were visible during revolution 127. Assuming that a large fraction of the X-ray emitting material is located above the starspots, a larger volume of emitting material was visible during revolution 210 that could explain the larger emission measure of "cool" (kT < 1 keV) plasma during this revolution (see Table 3). For hot (kT > 1 keV) plasma, it is more difficult to distinguish between rotationally modulated active regions and flares.

Assuming that UZ Librae is a K0 giant with a low mass secondary (Olah et al. 2002), a possible explanation of its high X-ray luminosity could be related to its binarity and evolutionary status. The outer convection zone of UZ Librae deepened since its evolution out of the main sequence, thus increasing its convective turnover time scale (Gilliland 1985). Since UZ Librae maintained a high rotation rate by tidal interaction with its close companion, its Rossby number (Durney & Latour 1978) decreased and dynamo activity increased as the star evolved towards the RGB. During this period, the deepening convective envelope may have suffered shear stresses, which could have resulted in radial velocity gradients, especially at the interface between the convection zone and the radiative core below it. The necessary conditions were then present to stimulate an α-Ω dynamo with an increasing efficiency. Our spectral analysis of the X-ray data suggests that the large fluid kinetic helicity induced by the rapid rotation currently generates magnetic fields with characteristic scales comparable with compact and with large interconnecting solar loops. The strong dynamo productive of this magnetic flux induces a high density of active regions covering a large fraction of the star surface. The X-ray emission would be strongly enhanced not only due to the occurrence of these magnetic structures, but mainly due to their large surface coverage and to their permanent interactions. These interactions lead to an uninterrupted flaring activity that generates large volumes of hot plasmas, thus explaining the high X-ray luminosity of the star.

Acknowledgements. We thank our colleagues from the *XMM–Newton* Science Operation Center for their support in implementing the observations. We are grateful to the anonymous referee for providing helpful comments on the manuscript.

References

Anders, E., & Grevesse, N. 1989, Geochim. Cosmochim. Acta, 53, 197
Antonucci, E., & Dodero, M. A. 1995, ApJ, 438, 480
Arnaud, K., & Dorman, B. 2001, XSPEC User's Guide for version 11.1, `http://heasarc.gsfc.nasa.gov/docs/xanadu/xspec/manual/manual.html`
Bambynek, W., Craseman, B., Fink, R. W., et al. 1972, Rev. Mod. Phys., 44, 716
Behar, E., Cottam, J., & Kahn, S. M. 2001, ApJ, 548, 966
Bopp, B. W., & Stencel, R. E. 1981, ApJ, 247, L131
Bopp, B. W., Goodrich, B., Africano, J., et al. 1984, ApJ, 285, 202
Brickhouse, N. S., Dupree, A. K., Edgar, R. J., et al. 2000, ApJ, 530, 387
Brinkman, A. C., Gunsing, C. J. T., Kaastra, J. S., et al. 2000, ApJ, 530, 111
Dempsey, R. C., Linsky, J. L., Fleming, T. A., et al. 1997, ApJ, 478, 358
den Herder, J. W., Brinkman, A. C., Kahn, S. M., et al. 2001, A&A, 365, L7
Dickey, J. M., & Lockman, F. J. 1990, ARA&A, 28, 215
Doschek, G. A., & Cowan, R. D. 1984, ApJS, 56, 67
Drake, S. A., Simon, T., & Linsky, J. L. 1989, ApJS, 71, 905
Dupree, A. K., Brickhouse, N. S., Doschek, G. A., et al. 1993, ApJ, 418, 41
Durney, B. R., & Latour, J. 1978, Geophys. Astrophys. Fluid Dyn., 9, 241
Ehle, M., Breitfellner, M., Dahlem, M., et al. 2001, The *XMM–Newton* Users' Handbook, `http://xmm.vilspa.esa.es/user/AO2/uhb/xmm_uhb.html`
Fekel, F. C., Strassmeier, K. G., Weber, M., et al. 1999, ApJS, 137, 369
Gabriel, A. H., & Jordan, C. 1969, MNRAS, 145, 241
Gilliland, R. L. 1985, ApJ, 299, 286
Gondoin, P., Aschenbach, B., Erd, C., et al. 2000, SPIE Proc., 4140, 1
Grewing, M., Bianchi, L., & Garrido, R. 1989, A&A, 123, 212
House, L. L. 1969, ApJS, 18, 2
Jansen, F., Lumb, D., Altieri, B., et al. 2001, A&A, 365, L1
Liedahl, D. A., Osterheld, A. L., & Goldstein, W. H. 1995, ApJ, 438, 115

Makishima, K. 1986, in The Physics of Accretion onto Compact Objects, 250, ed. K. O. Mason, M. G. Watson, & N. E. White (Berlin: Springer Verlag)
Mason, K. O., Breeveld, A., Much, R., et al. 2001, A&A, 365, L36
Mewe, R., Gronenschild, E. H. B. M., Heise, J., et al. 1982, ApJ, 260, 233
Mewe, R., Gronenschild, E. H. B., & van den Oord, G. H. J. 1985, A&A, 62, 197
Olah, K., Strassmeier, K. G., & Weber, M. 2002, A&A, 389, 202
Perryman, M. A. C., Lindegren, L., Kovalevsky, J., et al. 1997, A&A, 323, L49
Pradhan, A. K. 1982, ApJ, 263, 477
Raymond, J. C., & Smith, B. W. 1977, ApJS, 35, 419
Rosner, R., Tucker, W. H., & Vaiana, G. S. 1978, ApJ, 220, 643
Schrijver, C. J., Mewe, R., van den Oord, G. H. J., & Kaastra, J. S. 1995, A&A, 296, 477
Strassmeier, K. G. 1996, A&A, 314, 558
Strüder, L., Briel, U., Dennerl, K., et al. 2001, A&A, 365, L18
Tsuru, T., Makishima, K., Ohashi, T., et al. 1989, PASJ, 41, 679
Turner, M. J. L. T., Abbey, A., Arnaud, M., et al. 2001, A&A, 365, L27
Vaiana, G. S., Davis, J. M., Giacconi, R., et al. 1973, ApJ, 185, 47
Vaiana, G. S., & Rosner, R. 1978, ARA&A, 16, 393
van den Oordt, G. H. J, & Mewe, R. 1989, A&A, 213, 245
van Speybroeck, L. P., Krieger, A. S., & Vaiana, G. S. 1970, Nature, 227, 818
Wisniewski, W. Z. 1973, MNRAS, 161, 331